

Enhancement of Rydberg-mediated single-photon nonlinearities by electrically tuned Förster Resonances

H. Gorniaczyk,^{1,*} C. Tresp,¹ P. Bienias,² A. Paris-Mandoki,¹ W. Li,³
I. Mirgorodskiy,¹ H. P. Büchler,² I. Lesanovsky,³ and S. Hofferberth^{1,†}

¹*Phys. Inst. and Center for Integrated Quantum Science and Technology,
Universität Stuttgart, Pfaffenwaldring 57, 70569 Stuttgart, Germany*

²*Institute for Theoretical Physics III and Center for Integrated Quantum Science and Technology,
Universität Stuttgart, Pfaffenwaldring 57, 70569 Stuttgart, Germany*

³*School of Physics and Astronomy, University of Nottingham, Nottingham, NG7 2RD, United Kingdom*

We demonstrate experimentally that Stark-tuned Förster resonances can be used to substantially increase the interaction between individual photons mediated by Rydberg interaction inside an optical medium. This technique is employed to boost the gain of a Rydberg-mediated single-photon transistor and to enhance the non-destructive detection of single Rydberg atoms. Furthermore, our all-optical detection scheme enables high-resolution spectroscopy of two-state Förster resonances, revealing the fine structure splitting of high- n Rydberg states and the non-degeneracy of Rydberg Zeeman substates in finite fields. We show that the $|50S_{1/2}, 48S_{1/2}\rangle \leftrightarrow |49P_{1/2}, 48P_{1/2}\rangle$ pair state resonance in ^{87}Rb enables simultaneously a transistor gain $\mathcal{G} > 100$ and all-optical detection fidelity of single Rydberg atoms $\mathcal{F} > 0.8$. We demonstrate for the first time the coherent operation of the Rydberg transistor with $\mathcal{G} > 2$ by reading out the gate photon after scattering source photons. Comparison of the observed readout efficiency to a theoretical model for the projection of the stored spin wave yields excellent agreement and thus successfully identifies the main decoherence mechanism of the Rydberg transistor.

Rydberg excitations of ultracold atoms [1] are currently attracting tremendous attention because of possible applications in quantum computing [2–5] and simulation [6–10]. One particular aspect is the realization of few-photon nonlinearities mediated by Rydberg interaction [11–14], enabling novel schemes for highly efficient single-photon generation [15, 16], entanglement creation between light and atomic excitations [17], single-photon all-optical switches [18] and transistors [19, 20], and interaction-induced photon phase shifts [21]. Interacting Rydberg polaritons also enable attractive forces between single photons [22], crystallization of photons [23] and photonic scattering resonances [24].

The above experiments and proposals make use of the long-range electric dipole-dipole interaction between Rydberg atoms [25–27]. A highly useful tool for controlling the interaction are Stark-tuned Förster resonances, where two dipole-coupled pair states are shifted into resonance by a dc [28] or microwave [29, 30] electric field. Förster resonances have been studied by observation of dipole blockade [31], line shape analysis [32], double-resonance spectroscopy [33], excitation statistics [34], and Ramsey spectroscopy [35, 36]. Recently, the anisotropic blockade on Förster resonance [37] and quasi-forbidden Förster resonances [38] have been observed and Förster resonances between different atomic species have been predicted [39]. For Rydberg-mediated single-photon transistors, the near-resonance in zero field for specific pair states has been used to enhance the transistor gain [20], while in experiments on Rydberg atom imaging [40, 41] an increase in Rydberg excitation hopping has been observed on resonance [42].

In this work we use Stark-tuned Förster resonances to greatly increase the interaction between individual photons inside a Rydberg medium. We achieve this by tuning pair states $|S^{(g)}, S^{(s)}\rangle$ containing two different Rydberg S -states into resonance with $|P^{(g)}, P^{(s)}\rangle$ pair states by an electric field. We show that for gate and source Rydberg states $|50S_{1/2}, 48S_{1/2}\rangle$ we can boost the performance of a Rydberg single-photon transistor. When operated classically, we achieve $\mathcal{G} > 100$, enabling high-fidelity detection of single Rydberg atoms. This improved transistor can be operated coherently, reaching a gain $\mathcal{G} > 2$ when the gate photon is retrieved. We develop theoretical models for the dynamics of Rydberg polaritons in the presence of Förster resonances and the loss of coherence due to photon scattering. Excellent agreement with our experimental data is found. Finally, our all-optical probe represents a novel approach for the high-resolution study of the substructure of Förster resonances caused by fine structure and Stark/Zeeaman splitting of the $|P^{(g)}, P^{(s)}\rangle$ pair states. We demonstrate this technique by resolving the multi-resonance structure of the $|66S_{1/2}, 64S_{1/2}\rangle$ pair of states.

Our experimental scheme [13, 19, 20, 40] is shown in Fig. 1a,b: we first store a gate photon as a Rydberg excitation containing the state $|S^{(g)}\rangle$ inside a cloud of ultracold ^{87}Rb atoms. We then probe the presence of this gate excitation by monitoring the transmission of source photons coupled via electromagnetically induced transparency (EIT) to the source Rydberg state $|S^{(s)}\rangle$. At zero electric field, the interaction between the $|S^{(g)}, S^{(s)}\rangle$ pair is of van der Waals type. The difference in electric polarizability between S - and P -states enables the

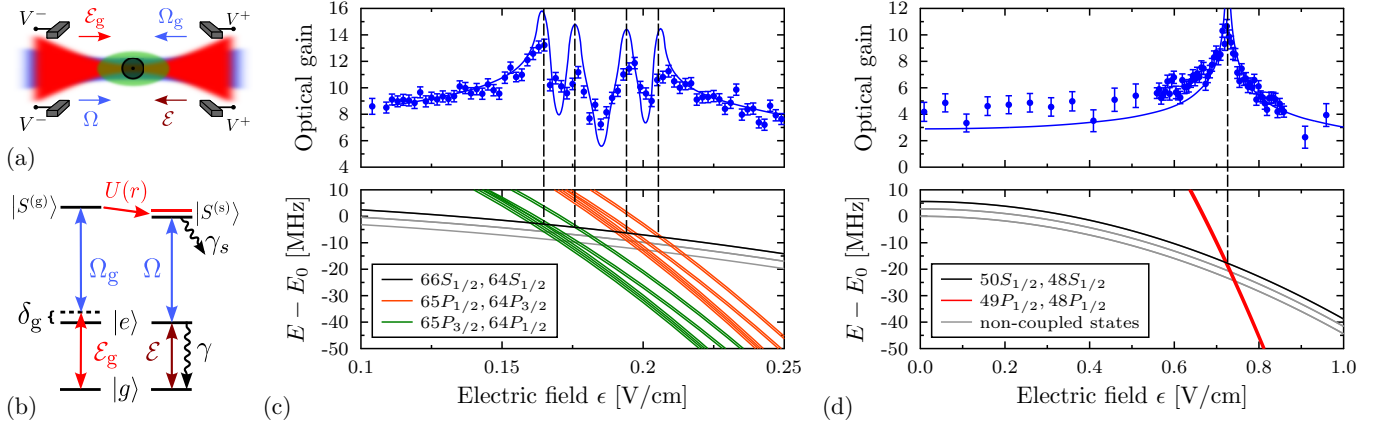


FIG. 1: (a) Tightly focussed source and gate beams ($w_0 = 6.2 \mu\text{m}$) are overlapped with an optically trapped cloud of 2×10^4 ^{87}Rb atoms at $3 \mu\text{K}$ (cylindrical $1/e$ dimensions $L = 40 \mu\text{m}$, $R = 10 \mu\text{m}$). For each transistor operation the optical trap is shut off for $200 \mu\text{s}$. We perform 23 individual experiments in a single cloud, recapturing the atoms in-between with minimal loss and heating. In-vacuum electrodes are used to apply the electric field. (b) Level scheme for gate and source photons coupled to different Rydberg states, where 2Ω is the Rabi frequency of the control field and 2γ is the decay rate of $|e\rangle$. (c,d) At certain electric fields (vertical dashed lines), the $|S^{(g)}, S^{(s)}\rangle$ pair state is resonant to pair states of type $|P^{(g)}, P^{(s)}\rangle$. The enhancement of interaction between $|S^{(g)}\rangle$ and $|S^{(s)}\rangle$ manifests in peaking of the transistor gain, visible in the blue data points. In (c), the fine structure of the involved P -states and the m_J -dependence of the Stark-shift result in the observed multi-resonance structure. The blue solid line is a theoretical analysis of the full polariton propagation in the presence of the gate excitation.

shift of the initial pair state into degeneracy with specific $|P^{(g)}, P^{(s)}\rangle$ pairs, resulting in resonant dipole-dipole interaction. We shift the Rydberg levels by applying a homogeneous electric field along the direction of beam propagation. Active cancellation of stray electric fields is done with 8 electric field plates in Löw configuration [43], while the homogeneous field results from additional voltages V^+, V^- to four electrodes (Fig. 1a).

We first study the pair state $|S^{(g)}, S^{(s)}\rangle = |66S_{1/2}, 64S_{1/2}\rangle$. Due to the fine structure splitting of the Rydberg P -states, this pair is near resonant with two P -state pairs $|65P_{1/2}, 64P_{3/2}\rangle$ and $|65P_{3/2}, 64P_{1/2}\rangle$ [20]. Both $|P^{(g)}, P^{(s)}\rangle$ pairs can be tuned into resonance at electric fields $\epsilon < 0.25 \frac{\text{V}}{\text{cm}}$. The full pair state Stark map in the presence of a magnetic field $B = 1 \text{ G}$ (Fig. 1c, gray lines) reveals a large number of closely spaced resonances arising from the non-degenerate $(m_J^{(g)}, m_J^{(s)})$ combinations. The strength of individual resonances depends on the angle θ between the interatomic axis and the quantization axis defined by the external fields, resulting in a non-spherical blockade volume [27]. We explore these resonances by measuring the optical gain

$$\mathcal{G} = \left(\bar{N}_{\text{s,out}}^{\text{no gate}} - \bar{N}_{\text{s,out}}^{\text{with gate}} \right) / \bar{N}_{\text{g,in}}, \quad (1)$$

i.e., the number of source photons scattered by a single incident gate photon [20], as a function of applied electric field (Fig. 1c). Our high-resolution spectroscopy indeed reveals four resonances, matching with the calculated crossings of different pair state groups. In between resonances, the coupling of $|S^{(g)}, S^{(s)}\rangle$ to multiple

$|P^{(g)}, P^{(s)}\rangle$ pair states with positive and negative Förster defects results in smaller blockade than in the zero-field case. This interplay between different resonances actually decreases the measured gain with respect to the field-free value. This situation does not occur for the Förster resonance $|50S_{1/2}, 48S_{1/2}\rangle \leftrightarrow |49P_{1/2}, 48P_{1/2}\rangle$ at $\epsilon = 0.710 \frac{\text{V}}{\text{cm}}$ (Fig. 1d). For this state combination there is one isolated resonance, resulting in the single peak in the optical gain.

To quantitatively describe the observed resonances we include in the microscopic description of polariton propagation [13, 14, 24] the special character of the interaction close to Förster resonance [44]. For illustration, we consider the $|50S_{1/2}, 48S_{1/2}\rangle$ pair and angle $\theta = 0$, which results in the selection rule $\Delta M_J = \Delta m_J^{(g)} + \Delta m_J^{(s)} = 0$ for the magnetic quantum numbers of the involved states. We then need to include four pair states: $\{|50S_{1/2}, 48S_{1/2}\rangle, |49P_{1/2}, 48P_{1/2}\rangle, |48P_{1/2}, 49P_{1/2}\rangle, |48S_{1/2}, 50S_{1/2}\rangle\}$ with $(m_J^{(g)}, m_J^{(s)}) = (\frac{1}{2}, \frac{1}{2})$. In this basis, the interaction Hamiltonian reduces to

$$H_{\text{dd}}(r) = \frac{1}{r^3} \begin{pmatrix} 0 & C_3 & C'_3 & 0 \\ C_3 & 0 & 0 & C'_3 \\ C'_3 & 0 & 0 & C_3 \\ 0 & C'_3 & C_3 & 0 \end{pmatrix} \quad (2)$$

with two dipolar coupling parameters C_3, C'_3 . Since the interaction is dominated by the Förster resonance, we neglect any residual van der Waals interactions. In general, the Hamiltonian (2) gives rise to flip-

flop (*hopping*) processes of type $|50S_{1/2}, 48S_{1/2}\rangle \rightarrow \{|49P_{1/2}, 48P_{1/2}\rangle, |48P_{1/2}, 49P_{1/2}\rangle\} \rightarrow |48S_{1/2}, 50S_{1/2}\rangle$. However, for this choice of Rydberg states the dipolar coupling parameters satisfy $C_3 \gg C'_3$, and therefore provide a strong suppression of hopping. This behavior is in contrast to the results in Ref. [42], where hopping processes strongly influenced the interaction mediated imaging of Rydberg excitations. In the experimentally relevant regime with $\omega, \gamma_s, \gamma_p \ll \Omega, \gamma$, where ω is the probe photon detuning, while γ_s and γ_p describe the decoherence rates of $|S^{(s)}\rangle$ and $|P^{(s)}\rangle$ excitations, the equation describing a single polariton $\mathcal{E}(r, \omega)$ and its interaction with the gate Rydberg excitation $|S^{(g)}\rangle$ at position r_j simplifies to

$$\left(ic\partial_r + \frac{g^2(\omega - i\gamma_s)}{\Omega^2} + \frac{g^2 V_{\text{ef}}^j(r)}{\Omega^2 - i\gamma V_{\text{ef}}^j(r)} \right) \mathcal{E}(r, \omega) = 0. \quad (3)$$

Here, $g = g_0 \sqrt{n_{\text{at}}}$ is the collective coupling strength with g_0 being the single atom-photon coupling strength and n_{at} is the atomic density. The effective interaction V_{ef}^j simplifies to

$$V_{\text{ef}}^j(r) = \frac{C_3^2}{\Delta_D - \omega - i\gamma_p} \frac{1}{(r - r_j)^6} \quad (4)$$

where Δ_D is the Förster defect. It is remarkable that, regardless of Δ_D , our microscopic derivation provides an effective interaction always based on van der Waals type interaction.

For comparison with experiment, we generalize our calculation to nonzero angles θ between the quantization and interatomic axis as well as to the larger number of states involved for the $|66S_{1/2}, 64S_{1/2}\rangle$ pair. We then integrate Eq. (3) over the cloud shape and average over the stored spin wave. We also take into account the Poissonian statistics of the gate and source photons, the storage efficiency, the fact that the blockade radius is comparable to the beam waist, and the finite experimental resolution in electric-field $\Delta\epsilon = \pm 2 \frac{\text{mV}}{\text{cm}}$ [44]. The comparison, without any free parameters, with experimental results for the gain is shown in Fig. 1. We find very good agreement for all electric fields except very close to the resonances. One reason for the discrepancy is the following: Close to the Förster resonance and for distances on the order of r_b between gate and source, the atomic part of the polariton-excitation pair initially in $|50S_{1/2}, 48S_{1/2}\rangle$ is converted into the superposition of $|49P_{1/2}, 48P_{1/2}\rangle$ and $|50S_{1/2}, 48S_{1/2}\rangle$. This results in additional slowing down of the polariton, and, consequently, an accumulation of polaritons close to r_b . Then, the assumption to study the propagation of individual polaritons breaks down as the interaction between the polaritons have to be included.

Next, we investigate to what extent these Förster resonances can be used to improve the Rydberg single photon transistor [19, 20]. We find that for this application, the $|50S_{1/2}, 48S_{1/2}\rangle$ resonance is ideal. It enables large source

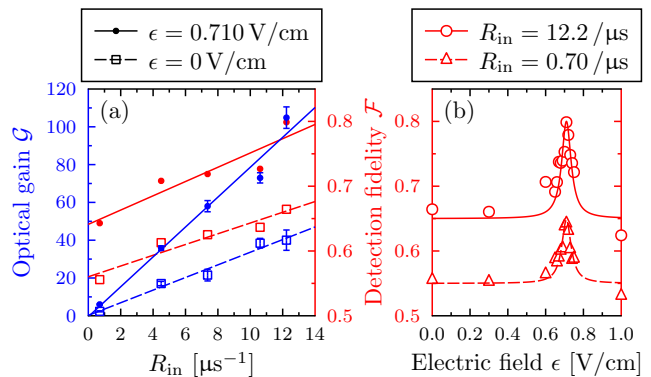


FIG. 2: Performance of the single-photon transistor on the $|50S_{1/2}, 48S_{1/2}\rangle \leftrightarrow |49P_{1/2}, 48P_{1/2}\rangle$ resonance. (a) Gain and single Rydberg detection fidelity increase linearly with the rate of incident source photons R_{in} in the nondestructive range where the creation of stationary excitations from source photons is negligible. Both the optical gain (a) and the single Rydberg detection fidelity (a,b) are highly amplified on the Förster resonance at $\epsilon = 0.710 \frac{\text{V}}{\text{cm}}$. The solid curves are linear or Lorentzian fits to guide the eye.

photon input rates, because of the relatively weak van der Waals interaction between source photons coupled to $|48S_{1/2}\rangle$. On the other hand, the Förster resonance provides sufficient gate-source interaction to observe high transistor gain. For source photon rate $R_{\text{in}} = 35 \mu\text{s}^{-1}$ we reach a maximal gain of $\mathcal{G} = 200$. At such high source rates we observe an accumulation of stationary Rydberg excitations in the medium, which we attribute to dephasing of single source polaritons. This effect has been previously observed for Rydberg S -states [14] and differs from the interaction-induced dephasing of D -state polariton pairs [45]. This accumulation sets an upper limit on the source photon rate for the non-destructive imaging of single Rydberg excitations [40], since the creation of additional Rydberg atoms also “destroys” the original system. We thus restrict our analysis in Fig. 2 to non-destructive source input rates for which the maximum temporal change in source transmission remains smaller than 10%. In this regime, we observe a linear increase of the optical gain with R_{in} both at zero electric field and on the Förster resonance (Fig. 2a). Exploiting the Förster resonance we can improve the optical gain by a factor > 2 on resonance (blue dots) compared to the zero field case (blue squares). The large number of source photons scattered from a single gate excitation enables the single shot detection of a stored gate photon with high fidelity [18, 19, 46]. In Fig. 2 we show this fidelity as a function of the applied electric field for two source photon rates. The Förster resonance enables a substantial increase of the fidelity to a maximal value of $\mathcal{F} = 0.8$. This number is mainly limited by the fact that our beam waist w_0 is slightly larger than the gate-source blockade distance. For spatially resolved Rydberg detection [40, 41], even

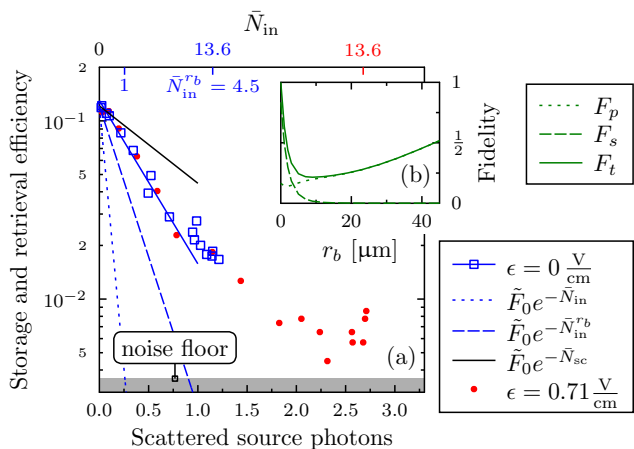


FIG. 3: (a) Efficiency of storing and reading out one single gate photon versus the number of scattered source photons during the storage time of $4.2\ \mu\text{s}$. When plotted as function of scattered photons, the observed retrieval efficiencies on Förster resonance (red dots) and in zero field (blue squares) are identical. (b) Calculated fidelity, i.e. the overlap between the initial gate spin-wave state and the final state after the propagation of a source photon through a one-dimensional Gaussian atomic cloud. The fidelity is the sum of contributions from scattered (short dashes) and transmitted (long dashes) source polaritons. The lines in (a) show the predicted decay of retrieval efficiency using the full propagation model (solid blue line) as well as different limiting cases (see main text for details).

higher fidelities are possible using imaging systems with better optical resolution than our beam size $w_0 = 6.2\ \mu\text{m}$.

The improved gate-source interaction on Förster resonance enables us for the first time to operate our transistor coherently by retrieving the stored gate photon after the transistor operation [46]. Without any source photon input, we measure a coherence lifetime of $3.6\ \mu\text{s}$ for stored gate photons, mainly limited by the finite temperature of our atomic sample. Next, we apply a source pulse containing a mean number of photons \bar{N}_{in} and pulse length $T = 3.2\ \mu\text{s}$ during a storage time of $4.2\ \mu\text{s}$. On Förster resonance, we achieve a mean number of scattered source photons within this time of up to 2.7 photons for a single stored gate photon (Fig. 3a). This is the first demonstration of a coherent transistor with gain $\mathcal{G} > 2$, a fundamental step towards quantum circuits employing feedback and gain or the non-destructive detection of the gate photon [47].

The overall fidelity of the transistor is limited by projection and dephasing of the gate spin-wave due to scattered and transmitted source photons [46, 48]. In Fig. 3a we show the absolute retrieval efficiency versus incident and scattered source photons at a mean number of $\bar{N}_{\text{g,in}} = 0.8$ incident gate photons on and off the Förster resonance. Interestingly, both cases collapse onto one exponential decay if plotted versus the number of scattered

source photons. The black curve in Fig. 3a assumes zero retrieval fidelity for one or more scattered source photons. Since the data lies below this limit, transmitted source polaritons must cause additional decoherence. On the other hand, the transmitted source photons do not completely destroy the gate spin-wave, since the measured retrieval efficiency lies well above the limits of total destruction due to all incident photons \bar{N}_{in} (dotted line) and photons incident on the blockade sphere $\bar{N}_{\text{in}}^{r_b}$ (dashed line).

For more quantitative analysis we follow Ref. [48], considering a one-dimensional model of the zero-field case for a single source photon passing through the atomic cloud with Gaussian density profile. The gate photon is stored in the initial spin-wave state $\hat{\rho}_i$ and interacts with source photons via the potential from Eq. (4). After the source photon has left the atomic cloud the state of the atomic ensemble is $\hat{\rho}_f$, and the quantum mechanical fidelity between the initial and final state is given by $F = [\text{Tr}|\sqrt{\hat{\rho}_i}\sqrt{\hat{\rho}_f}|]^2 = F_p + F_s$ [49]. Here, F_p accounts for transmitted and F_s for scattered source polaritons. Both contributions are shown in Fig. 3b as a function of the blockade radius $r_b = (\gamma C_6/\Omega^2)^{1/6}$ for our experimental parameters. For large blockade radii, F_p becomes negligible because source photons are rarely transmitted through the blockaded region. To describe the experimental 3D situation we average the fidelities from Fig. 3b over the spatial transversal distribution of gate and source photons. With this approach, we obtain the blue solid line in Fig. 3a, which is in very good agreement with our data, despite the rather crude simplifications of our model. We consider this as evidence for the assumed mechanisms for the spin-wave decoherence to be correct. By identifying the decoherence mechanisms, we can isolate the required improvements for a high-fidelity coherent Rydberg transistor: The blockade volume of a single gate excitation must be larger than the stored gate spin-wave to avoid the projection, while the optical depth OD_B inside the blockaded region must be large to prevent the dephasing due to transmitted photons. Meeting both requirements simultaneously is challenging due to limits on the atomic density because of Rydberg-ground state interaction [18, 50].

In conclusion, we have shown that Rydberg-mediated single-photon nonlinearities can be greatly enhanced by electrically tuned Förster resonances. By carefully choosing the employed Förster resonance we have simultaneously improved the Rydberg transistor gain and the fidelity of single Rydberg atom detection. We identify the $|50S_{1/2}, 48S_{1/2}\rangle \leftrightarrow |49P_{1/2}, 48P_{1/2}\rangle$ resonance in ^{87}Rb as ideal both for the Rydberg single-photon transistor and non-destructive imaging of Rydberg atoms [40, 41]. Exploiting this resonance, we have demonstrated the first coherent operation of the Rydberg transistor. Our quantitative analysis of the reduction of retrieval efficiency caused by source photons points the way towards high-

fidelity Rydberg-based photonic gates and transistors. Our polariton propagation theory correctly accounts for the enhanced source-gate interaction and is in excellent agreement with experiment. It also reveals unexpected and rich properties close to Förster resonances. This regime enables study of the transition from two- to many-body interaction and propagation with excitation hopping [42, 51]. The complexity of the resonances due to the Rydberg level structure provides a wide range of tuning options. The gate-source interaction can be reduced or even switched off completely between individual resonances. Similarly, the angular dependence of the interaction can be greatly varied by the external field. This provides a rich set of new tools for tailoring the interaction of photons coupled to different Rydberg states inside the medium.

We thank Johannes Schmidt for construction of the electric field control, Sebastian Weber for calculation of Rydberg potentials, and Christian Zimmer for contribution to the experiment. This work is funded by the German Research Foundation through Emmy-Noether-grant HO 4787/1-1 and within the SFB/TRR21. H.G. acknowledges support from the Carl-Zeiss Foundation. I.L. acknowledges funding from the European Research Council under the European Union's Seventh Framework Programme (FP/2007-2013) / ERC Grant Agreement No. 335266 (ESCQUMA), the EU-FET Grant No. 512862 (HAIRS), the H2020-FETPROACT-2014 Grant No. 640378 (RYSQ), and EPSRC Grant No. EP/M014266/1. W.L. is supported through the Nottingham Research Fellowship by the University of Nottingham and acknowledges access to the University of Nottingham HPC Facility.

* h.gorniaczyk@physik.uni-stuttgart.de

† s.hofferberth@physik.uni-stuttgart.de

- [1] M. Saffman, T. G. Walker, and K. Mølmer, *Rev. Mod. Phys.* **82**, 2313 (2010).
- [2] T. Wilk, A. Gaëtan, C. Evellin, J. Wolters, Y. Miroshnychenko, P. Grangier, and A. Browaeys, *Phys. Rev. Lett.* **104**, 010502 (2010).
- [3] L. Isenhower, E. Urban, X. L. Zhang, A. T. Gill, T. Henage, T. A. Johnson, T. G. Walker, and M. Saffman, *Phys. Rev. Lett.* **104**, 010503 (2010).
- [4] H. Weimer, M. Müller, I. Lesanovsky, P. Zoller, and H. P. Büchler, *Nature Phys.* **6**, 382 (2010).
- [5] Y.-Y. Jau, A. M. Hankin, T. Keating, I. H. Deutsch, and G. W. Biedermann, *Nature Physics* (2015).
- [6] P. Schauß, M. Cheneau, M. Endres, T. Fukuhara, S. Hild, A. Omran, T. Pohl, C. Gross, S. Kuhr, and I. Bloch, *Nature* **491**, 87 (2012).
- [7] P. Schauß, J. Zeiher, T. Fukuhara, S. Hild, M. Cheneau, T. Macrì, T. Pohl, I. Bloch, and C. Gross, *Science* **347**, 1455 (2015).
- [8] T. M. Weber, M. Hönig, T. Niederprüm, T. Manthey, O. Thomas, V. Guarrera, M. Fleischhauer, G. Barontini, and H. Ott, *Nature Physics* **11**, 157 (2015).
- [9] A. W. Glaetzle, M. Dalmonte, R. Nath, C. Gross, I. Bloch, and P. Zoller, *Phys. Rev. Lett.* **114**, 173002 (2015).
- [10] R. M. W. van Bijnen and T. Pohl, *Phys. Rev. Lett.* **114**, 243002 (2015).
- [11] I. Friedler, D. Petrosyan, M. Fleischhauer, and G. Kurizki, *Phys. Rev. A* **72**, 043803 (2005).
- [12] J. D. Pritchard, D. Maxwell, A. Gauguier, K. J. Weatherill, M. P. A. Jones, and C. S. Adams, *Phys. Rev. Lett.* **105**, 193603 (2010).
- [13] A. V. Gorshkov, J. Otterbach, M. Fleischhauer, T. Pohl, and M. D. Lukin, *Phys. Rev. Lett.* **107**, 133602 (2011).
- [14] T. Peyronel, O. Firstenberg, Q. Liang, S. Hofferberth, A. V. Gorshkov, T. Pohl, M. D. Lukin, and V. Vuletić, *Nature* **488**, 57 (2012).
- [15] Y. O. Dudin and A. Kuzmich, *Science* **336**, 887 (2012).
- [16] D. Maxwell, D. J. Szwer, D. Paredes-Barato, H. Busche, J. D. Pritchard, A. Gauguier, K. J. Weatherill, M. P. A. Jones, and C. S. Adams, *Phys. Rev. Lett.* **110**, 103001 (2013).
- [17] L. Li, Y. O. Dudin, and A. Kuzmich, *Nature* **498**, 466 (2013).
- [18] S. Baur, D. Tiarks, G. Rempe, and S. Dürr, *Phys. Rev. Lett.* **112**, 073901 (2014).
- [19] H. Gorniaczyk, C. Tresp, J. Schmidt, H. Fedder, and S. Hofferberth, *Phys. Rev. Lett.* **113**, 053601 (2014).
- [20] D. Tiarks, S. Baur, K. Schneider, S. Dürr, and G. Rempe, *Phys. Rev. Lett.* **113**, 053602 (2014).
- [21] V. Parigi, E. Bimbard, J. Stanojevic, A. J. Hilliard, F. Nogrette, R. Tualle-Brouiri, A. Ourjoumtsev, and P. Grangier, *Phys. Rev. Lett.* **109**, 233602 (2012).
- [22] O. Firstenberg, T. Peyronel, Q. Liang, A. V. Gorshkov, M. D. Lukin, and V. Vuletić, *Nature* **502**, 71 (2013).
- [23] J. Otterbach, M. Moos, D. Muth, and M. Fleischhauer, *Phys. Rev. Lett.* **111**, 113001 (2013).
- [24] P. Bienias, S. Choi, O. Firstenberg, M. F. Maghrebi, M. Gullans, M. D. Lukin, A. V. Gorshkov, and H. P. Büchler, *Phys. Rev. A* **90**, 053804 (2014).
- [25] K. Singer, J. Stanojevic, M. Weidemüller, and R. Côté, *Journal of Physics B: Atomic, Molecular and Optical Physics* **38**, S295 (2005).
- [26] A. Schwettmann, J. Crawford, K. R. Overstreet, and J. P. Shaffer, *Phys. Rev. A* **74**, 020701 (2006).
- [27] T. G. Walker and M. Saffman, *Phys. Rev. A* **77**, 032723 (2008).
- [28] M. D. Lukin, M. Fleischhauer, R. Cote, L. M. Duan, D. Jaksch, J. I. Cirac, and P. Zoller, *Phys. Rev. Lett.* **87**, 037901 (2001).
- [29] K. Afrousheh, P. Bohlouli-Zanjani, D. Vagale, A. Murgford, M. Fedorov, and J. D. D. Martin, *Phys. Rev. Lett.* **93**, 233001 (2004).
- [30] P. Bohlouli-Zanjani, J. A. Petrus, and J. D. D. Martin, *Phys. Rev. Lett.* **98**, 203005 (2007).
- [31] T. Vogt, M. Viteau, J. Zhao, A. Chotia, D. Comparat, and P. Pillet, *Phys. Rev. Lett.* **97**, 083003 (2006).
- [32] I. I. Ryabtsev, D. B. Tretyakov, I. I. Beterov, and V. M. Entin, *Phys. Rev. Lett.* **104**, 073003 (2010).
- [33] A. Reinhard, K. C. Younge, T. C. Liebisch, B. Knuffman, P. R. Berman, and G. Raithel, *Phys. Rev. Lett.* **100**, 233201 (2008).
- [34] A. Reinhard, K. C. Younge, and G. Raithel, *Phys. Rev. A* **78**, 060702 (2008).
- [35] J. Nipper, J. B. Balewski, A. T. Krupp, B. Butscher,

- R. Löw, and T. Pfau, *Phys. Rev. Lett.* **108**, 113001 (2012).
- [36] J. Nipper, J. B. Balewski, A. T. Krupp, S. Hofferberth, R. Löw, and T. Pfau, *Phys. Rev. X* **2**, 031011 (2012).
- [37] S. Ravets, H. Labuhn, D. Barredo, T. Lahaye, and A. Browaeys, *Phys. Rev. A* **92**, 020701 (2015).
- [38] B. Pelle, R. Faoro, J. Billy, E. Arimondo, P. Pillet, and P. Cheinet, ArXiv e-prints (2015), [arXiv:1510.05350](https://arxiv.org/abs/1510.05350).
- [39] I. I. Beterov and M. Saffman, *Phys. Rev. A* **92**, 042710 (2015).
- [40] G. Günter, M. Robert-de-Saint-Vincent, H. Schempp, C. S. Hofmann, S. Whitlock, and M. Weidemüller, *Phys. Rev. Lett.* **108**, 013002 (2012).
- [41] B. Olmos, W. Li, S. Hofferberth, and I. Lesanovsky, *Phys. Rev. A* **84**, 041607 (2011).
- [42] G. Günter, H. Schempp, M. Robert-de Saint-Vincent, V. Gavryusev, S. Helmrich, C. S. Hofmann, S. Whitlock, and M. Weidemüller, *Science* **342**, 954 (2013).
- [43] R. Löw, H. Weimer, J. Nipper, J. B. Balewski, B. Butscher, H. P. Büchler, and T. Pfau, *Journal of Physics B: Atomic, Molecular and Optical Physics* **45**, 113001 (2012).
- [44] *See the Supplemental Material for details on the derivation of the presented theory.*
- [45] C. Tresp, P. Bienias, S. Weber, H. Gorniaczyk, I. Mirgorodskiy, H. P. Büchler, and S. Hofferberth, *Phys. Rev. Lett.* **115**, 083602 (2015).
- [46] W. Chen, K. M. Beck, R. Bücker, M. Gullans, M. D. Lukin, H. Tanji-Suzuki, and V. Vuletić, *Science* **341**, 768 (2013).
- [47] A. Reiserer, S. Ritter, and G. Rempe, *Science* **342**, 1349 (2013).
- [48] W. Li and I. Lesanovsky, *Phys. Rev. A* **92**, 043828 (2015).
- [49] A. Uhlmann, *Reports on Mathematical Physics* **9**, 273 (1976).
- [50] A. Gaj, A. T. Krupp, J. B. Balewski, R. Loew, S. Hofferberth, and T. Pfau, *Nature Comm.* **5**, 4546 (2014).
- [51] W. Li, D. Viscor, S. Hofferberth, and I. Lesanovsky, *Phys. Rev. Lett.* **112**, 243601 (2014).

SUPPLEMENTAL MATERIAL

Photon propagation in the presence of a Rydberg excitation

For the sake of simplicity we explain our general method explicitly considering the $|50S_{1/2}, 48S_{1/2}\rangle$ pair state and angle $\theta = 0$ between the interatomic axis and the quantization axis. Our model system is a one-dimensional gas of atoms, whose electronic levels are given in Fig. 1(b) in the main text. The photon field $\hat{\mathcal{E}}(z)$ resonantly couples the groundstate $|g\rangle$ with the excited state $|e\rangle$, while 2Ω denotes the Rabi frequency of the control laser field coupling the $|e\rangle$ state with the Rydberg state $|S^{(s)}\rangle$. Following Ref. [13, 14, 24], we introduce operators $\hat{P}^\dagger(z)$ and $\hat{S}^\dagger(z)$ which generate the atomic excitations into the $|e\rangle$ and $|S^{(s)}\rangle$ states, respectively, at position z . In addition, comparing to Ref. [13, 14, 24] we include a more complex atomic level structure of the source and the gate excitations by defining $\hat{\mathcal{P}}^\dagger(z)$, $\hat{\mathcal{Z}}^\dagger(z)$ and $\hat{\mathcal{B}}^\dagger(z)$ which create excitations into $|P^{(s)}\rangle$, $|S^{(g)}\rangle$ and $|P^{(g)}\rangle$ states, respectively. All the operators $\hat{O}(z) \in \{\hat{\mathcal{E}}(z), \hat{P}(z), \hat{S}(z), \hat{\mathcal{P}}(z), \hat{\mathcal{Z}}(z), \hat{\mathcal{B}}(z)\}$ are bosonic and satisfy the equal time commutation relation, $[\hat{O}(z), \hat{O}^\dagger(z')] = \delta(z - z')$.

The microscopic Hamiltonian describing the propagation consists of three parts: $\hat{H} = \hat{H}_p + \hat{H}_{ap} + \hat{H}_a$. The first term describes the photon propagation in the medium and is defined as

$$\hat{H}_p = -ic \int dz \hat{\mathcal{E}}^\dagger(z) \partial_z \hat{\mathcal{E}}(z),$$

with the speed of light in vacuum c . The atom-photon coupling is described by

$$\hat{H}_{ap} = \int dz \left[-\frac{i\gamma}{2} \hat{P}^\dagger(z) \hat{P}(z) + g \hat{\mathcal{E}}(z) \hat{P}^\dagger(z) + \Omega \hat{S}^\dagger(z) \hat{P}(z) + g \hat{P}(z) \hat{\mathcal{E}}^\dagger(z) + \Omega \hat{P}^\dagger(z) \hat{S}(z) \right],$$

where 2γ is the decay rate of e -level, while g is the collective coupling of the photons to the matter. The interaction between Rydberg levels is described by

$$\hat{H}_a = \int dz' \int dz \left[\hat{\mathcal{P}}^\dagger(z) \hat{\mathcal{B}}^\dagger(z') V(z - z') \hat{\mathcal{Z}}(z') \hat{S}(z) + \frac{\Delta_D}{2} \hat{\mathcal{P}}^\dagger(z) \hat{\mathcal{B}}^\dagger(z') \hat{\mathcal{B}}(z') \hat{P}(z) + \text{H.c.} \right],$$

where $V(z) = C_3/z^3$ is the dipolar interaction potential and Δ_D the Förster defect. Note, that for the experimental parameters $C_3 \gg C'_3$ and therefore it is sufficient to include in the interaction Hamiltonian only the C_3/z^3 coupling term. In addition, it follows that hopping of excitations is quenched, and therefore the $|S^{(g)}\rangle$ excitation is at a fixed position. Then, the description of a single photon propagation requires four components of the wave function: $\mathcal{E}\mathcal{Z}(z, t)$, $P\mathcal{Z}(z, t)$, $S\mathcal{Z}(z, t)$ and $\mathcal{P}\mathcal{B}(z, t)$, which denote the probability of finding the source excitation in \mathcal{E} , $|e\rangle$, $|S^{(s)}\rangle$ or $|P^{(s)}\rangle$ state at position z and the gate excitation in $|S^{(g)}\rangle$ or $|P^{(g)}\rangle$ state at the position z_j . The Schrödinger equation reduces to

$$\partial_t \mathcal{E}\mathcal{Z}(z, t) = -c \partial_z \mathcal{E}\mathcal{Z}(z, t) + ig P\mathcal{Z}(z, t), \quad (5a)$$

$$\partial_t P\mathcal{Z}(z, t) = -\frac{\gamma}{2} P\mathcal{Z}(z, t) + ig \mathcal{E}\mathcal{Z}(z, t) + i\Omega S\mathcal{Z}(z, t), \quad (5b)$$

$$\partial_t S\mathcal{Z}(z, t) = -iV_j(z) \mathcal{P}\mathcal{B}(z, t) + i\Omega P\mathcal{Z}(z, t), \quad (5c)$$

$$\partial_t \mathcal{P}\mathcal{B}(z, t) = -iV_j(z) S\mathcal{Z}(z, t) - i\Delta_D \mathcal{P}\mathcal{B}(z, t), \quad (5d)$$

where $V_j(z) = V(z - z_j)$. We solve the above set of coupled equations via Fourier transform in time, which leads to the equation for the photon field:

$$\left(-ic \partial_r - \frac{g^2 \left(V_{\text{ef}}^j(r) - \omega - i\gamma_s \right)}{-i\gamma\omega + (\gamma - i\omega)\gamma_s - \omega^2 + \Omega^2 - V_{\text{ef}}^j(r)(\omega + i\gamma)} - \omega \right) \mathcal{E}\mathcal{Z}(r, \omega) = 0, \quad (6)$$

with

$$V_{\text{ef}}^j(r) = \frac{C_3^2}{\Delta_D - \omega - i\gamma_p} \frac{1}{(r - r_j)^6}. \quad (7)$$

In the limit of $\gamma_s, \gamma_p \ll \Omega, \gamma$, these expressions simplify to the equations (3) and (4) from the main part of the Letter.

The equation for the \mathcal{E} -field can be generalized to the second pair of states $|66S_{1/2}, 64S_{1/2}\rangle$ by redefining the expression for $V_{\text{ef}}^j(r)$ to

$$V_{\text{ef}}^j(r) = \sum_{\alpha} \frac{C_{3,\alpha}^2}{\Delta_D^{\alpha} - \omega - i\gamma_p} \frac{1}{(r - r_j)^6} \quad (8)$$

where we sum over all relevant pairs of states α , which for $\theta = 0$ are

$$\alpha \in \{ |65P_{1/2}, m_J = 1/2, 64P_{3/2}, m_J = 1/2\rangle, |65P_{1/2}, m_J = -1/2, 64P_{3/2}, m_J = 3/2\rangle, \\ |65P_{3/2}, m_j = 1/2, 64P_{1/2}, m_j = 1/2\rangle, |65P_{3/2}, m_j = 3/2, 64P_{1/2}, m_j = -1/2\rangle \}.$$